Transition probabilities in ^{134}Pr: A test for existence of chirality in real nuclei

D. Tonev[1,2]

[1] Institute of Nuclear Research and Nuclear Energy, Bulgarian Academy of Sciences, 1784 Sofia, Bulgaria
[2] INFN, Laboratori Nazionali di Legnaro, I-35020 Legnaro, Italy

Abstract. Exited states in ^{134}Pr were populated in the fusion-evaporation reaction ^{119}Sn(^{19}F, 4n)^{134}Pr. Recoil distance Doppler-shift and Doppler-shift attenuation measurements using the Euroball spectrometer, in conjunction with the inner BGO ball and the Cologne plunger, were performed at beam energies of 87 MeV and 83 MeV, respectively. Reduced transition probabilities in ^{134}Pr are compared to the predictions of the two quasiparticle+triaxial rotor and interacting boson fermion-fermion models. The experimental results do not support the presence of static chirality in ^{134}Pr underlying the importance of shape fluctuations. Only within a dynamical context the presence of intrinsic chirality in ^{134}Pr can be supported.

1 Introduction

Chirality has recently been proposed as a novel feature of rotating nuclei [1–3]. A spontaneous breaking of the chiral symmetry can take place for configurations where the angular momenta of the valence protons, valence neutrons and the core are mutually perpendicular. This can occur, for example, when the proton and neutron Fermi levels are located in the lower part of valence proton high-j (particle-like) and in the upper part of valence neutron high-j (hole-like) subshells, and the core is triaxial. Under such conditions the angular momenta of the valence particles are aligned along the short and long axes of the triaxial core, while the angular momentum of the rotational core is aligned along the intermediate axis. The non zero components of the total angular momentum on all the three axes can form either a left-handed or a right-handed set and therefore, the system manifests chirality [2]. Since the chiral symmetry is dichotomic, its spontaneous breaking by the axial angular momentum vector leads to doublets of closely lying rotational bands of the same parity [1–3].

Recently, pairs of bands possibly due to the breaking of the chiral symmetry have been found in the mass A$\sim$130 region where the proton Fermi surface is positioned in the lower part and the neutron surface in the higher part of the $h_{11/2}$ subshell. The first example of two nearly degenerate bands with the same parity and spins has been reported for ^{134}Pr [4,5]. The two bands are displayed in Fig. 1. The degeneracy between levels of the same spin and parity is increasing with increasing spin and the bands cross above I $> 15\hbar$. In the context of chiral symmetry such a doublet

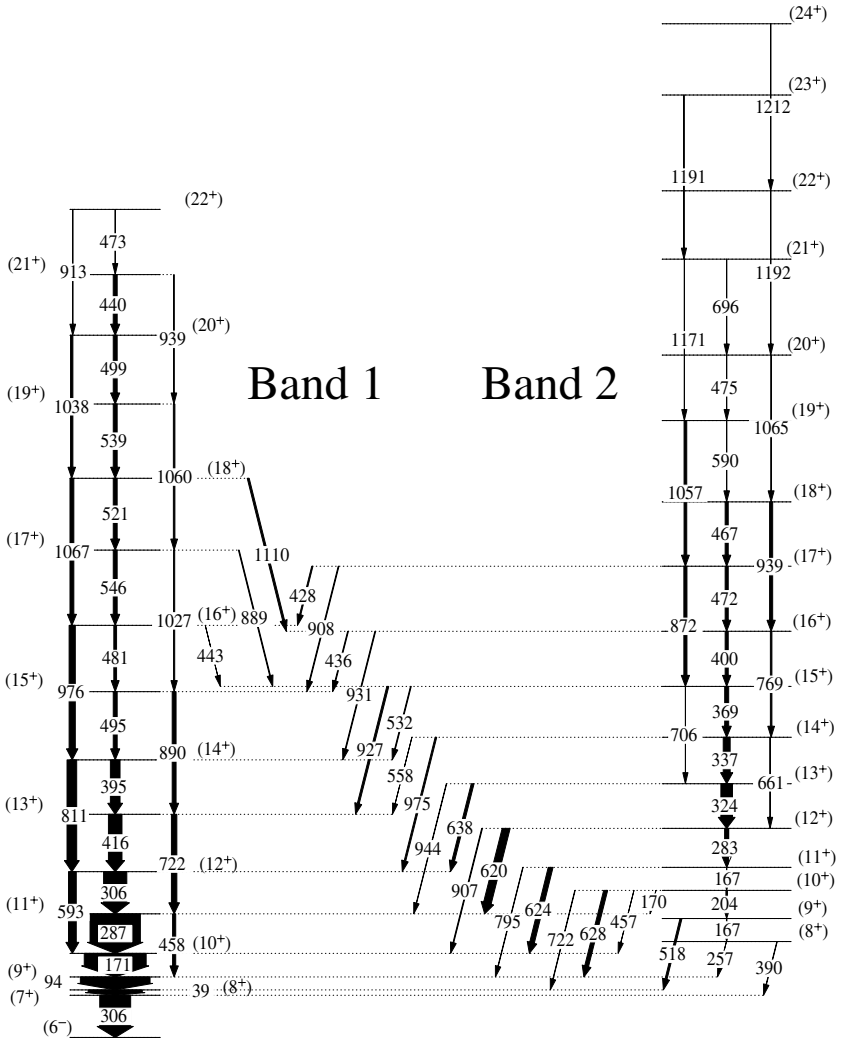

Figure 1. Partial level scheme of ^{134}Pr from Ref. [6]. Two nearly degenerate positive-parity bands, candidates for chiral partner bands, are indicated as Band 1 and Band 2.

of bands has been described within the framework of the particle-core coupling model [1, 3] and the tilted-axis cranking model [2]. An alternative interpretation has been based on the interacting boson fermion-fermion model (IBFFM) [7]. Here the energy degeneracy is also obtained but a different nature is attributed to the two bands. The yrast band is basically built on the ground state configuration of the triaxial core whereas the collective structure of the yrare band contains a large component of the γ-band and, with increasing angular momentum, of higher-lying collective core structures.

In order to confirm or reject the hypothesis of nuclear chirality, next to establish the existence of almost degenerate rotational bands, it is necessary to measure also other observables and compare them to the model predictions. Critical experimental observables for the understanding of nuclear structure and for checking the reliability of theoretical models are the electromagnetic transition probabilities. The aim of the present work is to investigate the electromagnetic transition probabilities in the doublet bands of ^{134}Pr.

2 Experiment, analysis, results

To measure lifetimes of excited states in ^{134}Pr by using the recoil distance Doppler-shift (RDDS) and Doppler-shift attenuation (DSA) measurements, the fusion-evaporation reaction ^{119}Sn(^{19}F, 4n) at beam energies of 87 and 83 MeV, respectively, was used. The beam was delivered by the Vivitron accelerator at IReS in Strasbourg. For the RDDS measurement, the target consisted of 0.5 mg/cm^2 ^{119}Sn foil enriched to 89.8 %. It was evaporated on a 1.8 mg/cm^2 ^{181}Ta foil facing the beam. A 6.0 mg/cm^2 Gold foil was used to stop the recoils which were leaving the target with a mean velocity of 0.98(2) % of the velocity of light, c. For the DSAM measurement, the target consisted of 0.7 mg/cm^2 ^{119}Sn evaporated onto a 9.5 mg/cm^2 ^{181}Ta backing used to stop the recoils. The γ-rays deexciting the recoiling ^{134}Pr nuclei were detected using the EUROBALL IV [8] detector array composed of 26 clover and 15 cluster Ge detectors and an inner BGO (Bismuth Germanate) ball. The cluster and clover detectors of EUROBALL were grouped into 10 rings corresponding to approximately the same polar angle with respect to the beam axis, namely ring 1 (θ=72.2°), ring 2 (θ=80.9°), ring 3 (θ=99.0°), ring 4 (θ=107.4°), ring 5 (θ=122.6°), ring 6 (θ=130.4°), ring 7 (θ=137.6°), ring 8 (θ=147.5°), ring 9 (θ=156.1°) and ring 10 (θ=163.5°). For the present RDDS and DSAM measurements, the rings of main interest are those where appreciable Doppler shifts can be observed, i.e. rings 5, 6, 7, 8, 9, 10. In the lifetime analysis, data only from one forward ring, namely ring number 1, were used. The trigger condition for data acquisition was set such that events were recorded when at least three γ-rays in the Ge cluster or clover segments and three γ-rays of the inner ball were in prompt coincidence. With such trigger conditions, the yield of ^{134}Pr was estimated to be 28% of the total cross-section. Gain matching and efficiency calibration of the Ge detectors were performed using ^{133}Ba, ^{152}Eu and ^{56}Co radioactive sources. A standard add-back correction for Compton scattering was applied. For the RDDS measurement, data were taken at 20 target-to-stopper distances ranging from electrical contact to 2500 μm. Some of the investigated transitions have low energies, and since v/c is 0.98(2) %, the resulting Doppler-shift is relatively small. For this reason, in the analysis, only detectors with good resolution were selected in order to obtain better line-shapes. The good statistics for the low lying states of ^{134}Pr allowed to construct γ-γ coincidence matrices in which the angular information is conserved on both axes. For the higher lying states of ^{134}Pr, because of the weaker statistics, only matrices were constructed where one of the axes was associated with a specific

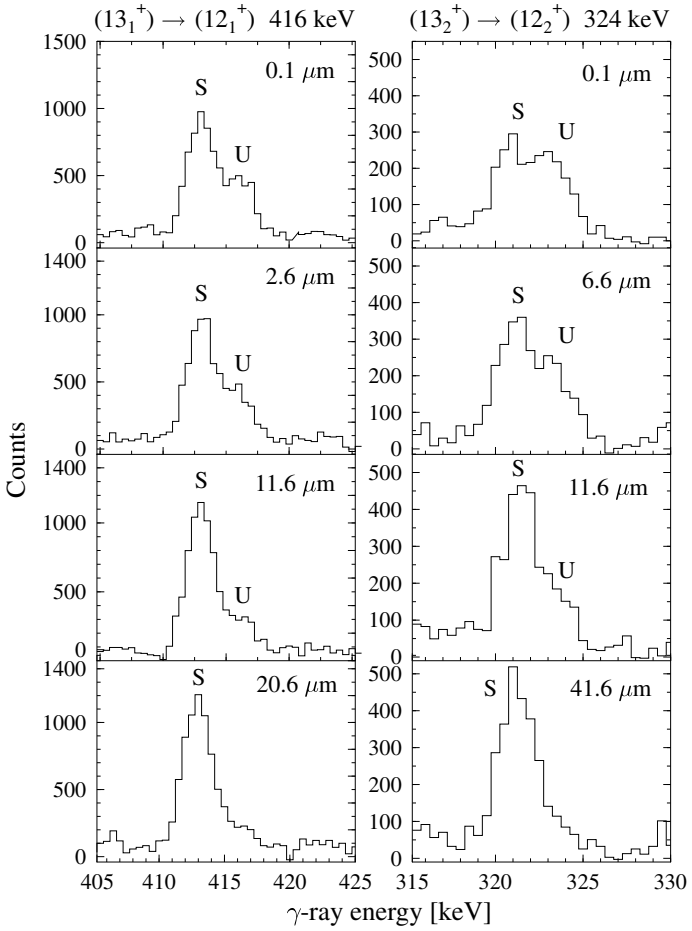

Figure 2. Gated γ-ray spectra of ^{134}Pr taken at four different distances. Summed spectra from all detectors at a backward angle of 137.60° with respect to the beam axis are shown. On the left-hand side, both shifted and unshifted peaks of the $13_1^+ \rightarrow 12_1^+$ transition are presented. On the right-hand side, the shifted and unshifted peaks of the $13_2^+ \rightarrow 12_2^+$ transition are shown. At the distance 41.6 μm, the transition 323.6 keV ($13_1^+ \rightarrow 12_2^+$) is fully shifted, while the transition 416.2 keV ($13_1^+ \rightarrow 12_1^+$) has only a shifted component already at the distance of 20.6 μm.

detection angle while on the other axis every detector (ring) firing in coincidence was allowed. For the RDDS case the normalization of the data taken at different target-to-stopper distances was performed using coincidence events corresponding to pairs of strong transitions. The level-scheme of ^{134}Pr obtained from the present data is reported in Fig. 1. Examples of spectra taken at different distances for two γ-ray transitions in ^{134}Pr are shown in Fig. 2.

For the analysis of the RDDS data, the standard version of the Differential decay-curve method (DDCM) [9] has been employed, with gates set on both shifted

(S) and unshifted (U) components of a transition depopulating levels below the level of interest. For each flight time t, a lifetime value τ for the level of interest is calculated by directly using the areas of the U or S peaks of a transition depopulating the investigated level and of the directly feeding transitions. A lifetime value is derived at each distance and the final result for τ is determined as an average of such values within the sensitivity region of the data. More details about the DDCM applied to RDDS measurements can be found in Refs. [9, 10]. For the analysis of the DSAM data, we performed a Monte-Carlo simulation of the slowing-down histories of the recoils using a modified [11,12] version of the program DESASTOP [13]. The analysis of the lineshapes was carried out according to the DDCM for treating DSAM data [10, 11]. The lifetimes of the levels with I^{π} from 10_1^+ to 18_1^+ and with I^{π} from 13_2^+ to 17_2^+ have been deduced. Except for the lifetime of the I^{π} =10_1^+ level [14], all the others are determined for the first time. We observe an excellent agreement with the lifetime value for the I^{π} =10_1^+ state reported in Ref. [14]. The results are shown in the Table 1.

Table 1. Derived lifetimes in Band 1 and Band 2 of ^{134}Pr. The used experimental technique is also indicated.

Band 1			Band 2	
State [I^{π}]	τ [ps]		State [I^{π}]	τ [ps]
10_1^+	4.93(15)	RDDS	13_2^+	1.443(50)
11_1^+	1.614(326)	RDDS	14_2^+	1.280(50)
12_1^+	1.425(130)	RDDS		
13_1^+	0.904(50)	RDDS		
14_1^+	0.882(147)	DSAM	15_2^+	0.887(47)
15_1^+	0.608(68)	DSAM	16_2^+	0.824(52)
16_1^+	0.562(47)	DSAM	17_2^+	0.353(49)
17_1^+	0.422(30)	DSAM		
18_1^+	0.249(10)	DSAM		

The lifetimes for the states 14_1^+ and 15_2^+ have been determined from both the RDDS and DSAM measurements. The results show very good agreement within the error. In the table we report only the DSAM results due to their higher statistical significance. Almost all branching ratios reported in Ref. [4] were revised. The clover rings of Euroball form a highly efficient Compton polarimeter. We confirmed that the delayed component of the 306 keV doublet has an E1 character as already reported by Roberts et al. [15]. On the basis of DCO [4] and linear polarization analysis, a M1 character with a negligible E2 component was assigned to the Δ I = 1 intraband transitions. The Δ I = 2 intraband and interband transitions show an E2 character. Details of the lifetime analysis, branching ratios and linear polarizations coefficients are reported in Refs. [16, 17].

3 Discussion

Reduced transition probabilities obtained from the present experiment are shown in Fig. 3. Within the experimental uncertainties, the B(M1) values in both partner bands behave similarly and point to relatively strong transition strengths. In contrast, the intraband B(E2) strengths within the two bands differ. In the angular-momentum region where the almost degeneracy of the energy levels of the two bands occurs (I^{π} = 14^{+} - 19^{+}), the B(E2) values for Band 1 are a factor 2 to 3 larger than those of Band 2. The B(M1)/B(E2) ratios obtained from the lifetime data are in a good agreement with the results extracted from intensity values reported in Ref. [4] and differ only for the I^{π} = 13^{+}_{1} and 15^{+}_{1} states from the values reported in Ref. [6]. In all measurements the corresponding B(M1)/B(E2) ratios for the two bands are different. The staggering in Band 1 reported in Ref. [6] is not observed in our data as well as in the data of Ref. [4]. Our results are incompatible with the pure chiral picture (static chirality) where the intraband B(E2) transition strengths must be almost equal [1, 19]. Such a finding points to the fact that the limit of static chirality is not reached in ^{134}Pr and the nucleus stays in a very soft vibrational regime.

In order to investigate the effects of the shape fluctuations we have compared the experimental transition strengths of the two bands with calculated ones by means of the two quasiparticle + triaxial rotor model (TQPTR) as described in [1, 20] and by the IBFFM [7]. For the TQPTR, the ratios between the moments of inertia have been calculated by cranking about the three principal axes using the parameters reported in Ref. [2], which gave $\mathcal{J}_s : \mathcal{J}_i : \mathcal{J}_l = 1.52 : 3.55 : 1$. In the IBFFM calculation, the proton and neutron were coupled to the triaxial core as described in Ref. [7]. Both descriptions include the coupling between the odd particles and the even-even core in a similar way, taking into account the partial filling of the $h_{11/2}$ shells. In the TQPTR model, a rigid triaxial shape is assumed for the core and the orientation in space is the only core degree of freedom. The IBFFM takes into account the deformation of the core as an additional degree of freedom. As discussed in [7], a cubic term had to be added to the standard IBA Hamiltonian in order to reproduce the energy spectra of ^{134}Pr and its even-even isobar ^{134}Ce. This term generates a triaxial equilibrium deformation. The fluctuations of the shape around this value are taken into account and their magnitude is fixed by adjusting the parameters for the IBA Hamiltonian to the data for ^{134}Ce. The results of both calculations are shown in Fig. 3. The comparison with the experimental data show a clear disagreement with the TQPTR results whereas a much better matching is found with the IBFFM calculation. Such result indicates that shape fluctuations are an essential ingredient for the proper description of the structure of the two bands [16, 17].

It is interesting to note that the difference of the transition strengths of the two bands is larger, and the theoretical values are closer to the experimental B(E2) values in the IBFFM calculation than in the TQPTR one. This fact supports the interpretation of Ref. [7] where the yrast band contains predominantly the ground state configuration of the triaxial core whereas the yrare band contains a major component of the γ-band. Such interpretation does not necessarily contradict the chiral

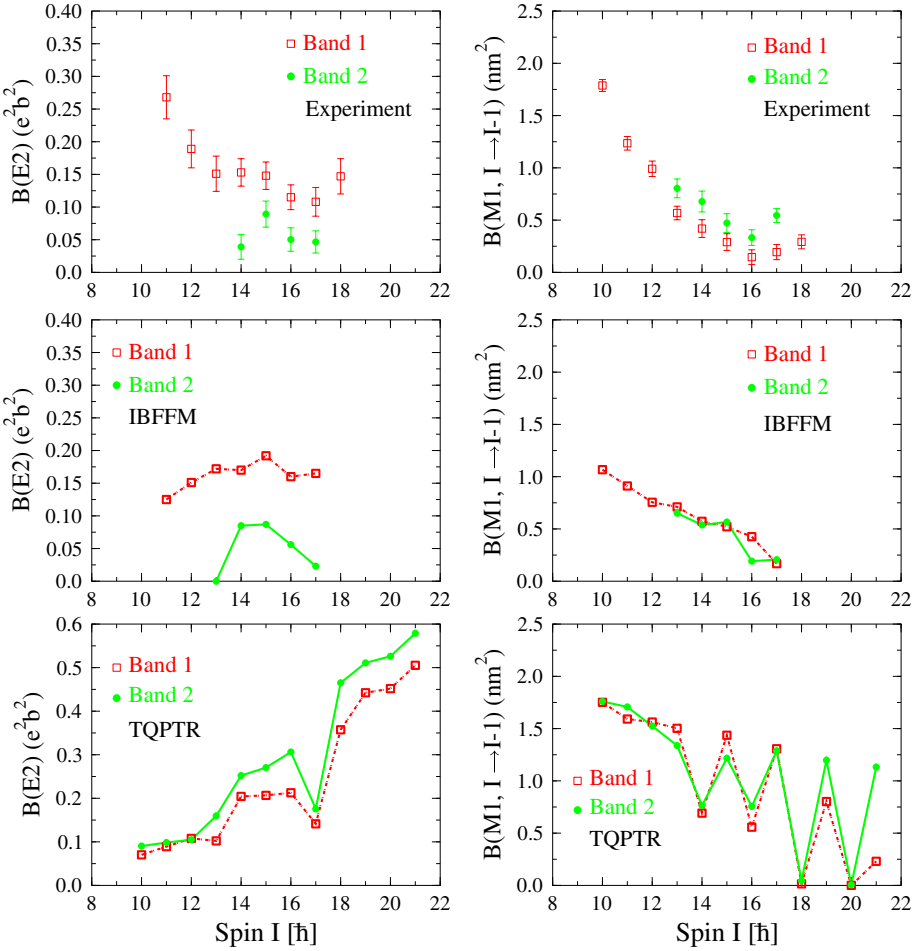

Figure 3. Experimentally determined and theoretically calculated B(E2) and B(M1) transition strengths in chiral candidate bands of ^{134}Pr. In the upper panels are presented experimental B(E2) and B(M1) values for transitions in Band 1 and Band 2. In the second row, the results of TQPTR calculations are displayed. In the panels on bottom are presented the predictions of the IBFFM.

interpretation, because the TQPTR calculations in Ref. [18] found a similar composition.

In the chiral interpretation the eigenstates of the Hamiltonian representing the two observed bands can be described as linear combinations of the wave functions in the left-handed and right-handed sectors. In the case of static chirality the overlap between the wave functions in the two sectors is weak. Because such coupling represents the tunneling between the two chiral configurations, the matrix elements of the electromagnetic transition operators between the two chiral sectors are expected to

be very small. Since the left- and right-handed components enter with equal weight into the two eigenstates, which differ only in the relative phase of the mixing amplitudes, the transition matrix elements of the two doublet bands have to be equal. In the case of dynamic chirality, the overlap between the wave functions of the two sectors is large. In such a condition there are large matrix elements of the transition operators that connect the left- to the right-handed sector. Due to orthogonality, these matrix elements enter the transition matrix elements of the eigenstates with opposite sign and make the transition strengths of the two doublet bands different.

The TQPTR calculation shows a transition from dynamic to static chirality with increasing spin. Below $I^{\pi} = 12^{+}$, the angular momentum vector oscillates between the left- and right-handed sectors, separated by the plane defined by the short and long axes(s-l). The two bands are well separated, representing the ground and first excited states of this chiral vibration [5]. Above $I^{\pi} = 12^{+}$, the angular momentum increases by adding core angular momentum perpendicular to the s-l-plane. This reduces the probability of the angular momentum vector to be near the s-l-plane, which makes the electromagnetic transition matrix elements between the two sectors small. Static chirality is approached, which is reflected by the two partner bands coming close together. The B(E2) values indicate that there is still a substantial tunneling between the two sectors. In the IBFFM model, the fluctuations of the triaxiality parameter γ around its mean value of 30^{o} admix near-axial shapes, which are achiral. This additional left-right coupling strongly increases the difference between the intraband B(E2) values. A pronounced staggering of the B(M1) values appears above $I^{\pi} = 12^{+}$ in the TQPTR model. An explanation for this staggering was given in Ref. [19] for the symmetric case where the angular momenta of the proton and the neutron hole are equal, the moments of inertia of the l- and s- axes are equal, and the left-right transition matrix element is negligible. Our TQPTR calculation does not strictly obey these conditions, mainly because the microscopic moments of inertia of the long and short axes are different. The staggering is absent in the data as well as in the results of the IBFFM calculations, which indicates that the additional left-right coupling caused by the shape fluctuations cancels the staggering effect forseen in [19].

The assumption of a constant deformation of γ=30^{o} in the TQPTR gives increasing B(E2) transition strengths as a function of spin, which is in contrast to the observed trend. Such an increase of the B(E2) transition strengths is directly related to the chiral geometry, which at low spins requires that the rotational axis lies in the plane defined by the short and long axes of the core, with an angle of 45^{o} with respect to both of them. In such a situation the B(E2) values are equal to zero. With increasing spin the angular momentum moves out of the plane which correspondingly increases the B(E2) values. For axial shape instead the same geometry gives rise to large B(E2) values. Therefore, the admixture of near axial shapes will increase the B(E2) values at low spin, which results in the almost constant values seen in Fig. 3 and foreseen by the IBFFM calculations.

4 Conclusions

Lifetimes in the two chiral candidates bands in ^{134}Pr were measured by means of the Recoil distance Doppler-shift and Doppler-shift attenuation method. The branching ratios and Electric or Magnetic character of the transitions were also investigated. We have determined the electromagnetic transition probabilities for the two bands in ^{134}Pr, which have been suggested to be chiral partners. In order to judge to what extend this interpretation is supported by our measurements we applied two theoretical models, TQPTR and IBFFM. Both models couple a $h_{11/2}$ particle-like quasiproton and a $h_{11/2}$ hole-like quasineutron to the even-even core. In the case of the TQPTR the core is a rigid triaxial rotor, the deformation of which and its moments of inertia were calculated by means of the TAC mean field theory. The TQPTR takes into account only the orientation of the angular momenta of the particle, of the hole, and of the core. The TQPTR describes very well the energies of the two bands, in particular the conspicuous sharp crossing between the two bands. However there are two discrepancies concerning the electromagnetic transition probabilities: i) The calculated inband B(E2) values are about the same for both bands, whereas the measured ones differ by a factor of two. ii) The calculations give strong B(M1) (and unstretched B(E2)) values which alternate with spin between inband and interband transitions, whereas the experimental inband values are large and the interband values are small.

The IBFFM core has the deformation parameters as additional degrees of freedom, which are described by the Interacting Boson Model. Since the standard boson IBM-1 Hamiltonian with one- and two-body interactions encompasses only the case of γ-instability, we have included three body boson terms in the Hamiltonian, which induce triaxiality. Adjusting the parameters to the even-even neighbors, the potential energy surface has a minimum around $\gamma = 20^o$, which is very shallow in the γ-direction and also rather broad in the β-direction. The γ-decay properties of levels in ^{134}Pr, calculated in this framework, are in excellent agreement with experimental data [17, 21]. However, the calculated energy splitting between the two bands is too large. The observed crossing between the two bands at I = 15 cannot be reproduced.

We analyzed the structure of the wave functions by calculating distributions of the mutual angles between the proton, neutron and core angular momenta, their triple product (orientation parameter), and the deformation parameters [17, 21]. At low spin, the TQPTR distributions have the character of a zero and one phonon state of a chiral vibration. At larger spin, where the bands cross, the two distribution become very similar, as expected for static chirality. However, the substantial presence of achiral configurations indicates that the chirality is dynamic, i. e. some slow, strongly anharmonic excursion of the angular momentum vector into the left- and right-handed sectors. The IBFFM distributions show a similar trend, but the transition is not as clearly visible. The presence of configurations with the angular momenta of the proton, neutron and core in the favorable, almost orthogonal geometry, is substantial but far from being dominant. There are large fluctuations of the deformation parameters β and γ around the triaxial equilibrium shape, which enhance the content of achiral configurations in the wavefunction.

The present study suggests that the existence of the two crossing ΔI = 1 bands with the same parity in ^{134}Pr should be attributed to a weak fluctuation dominated chirality combined with an intrinsic symmetry yet to be revealed.

Acknowledgments

D.T. express his gratitude to Ivanka Necheva for her outstanding support. This research has been supported by a Marie Curie Fellowship under contract number HPMF-CT-2002-02018, by the European Commission through contracts numbers HPRI-CT-1999-00078 and RII3-CT-2004-506065, by the BMBF under contract number 06K167 and by the US Department of Energy by the contract numbers DE-FG02-95ER40934 and DE-FG02-96ER40983. D.T. and P.P. are indebted to the National Science Fund at the Bulgarian Ministry of Education and Science for a financial support under contract number RIC-02/2007

References

1. S. Frauendorf et al., *Nucl. Phys. A* **617**, (1997) 131.
2. V. I. Dimitrov et al., *Phys. Rev. Lett.* **84**, (2000) 5732.
3. K. Starosta et al., *Nucl. Phys. A* **682**, (2001) 375c.
4. C. M. Petrache et al., *Nucl. Phys. A* **597**, (1996) 106.
5. K. Starosta et al., *Phys. Rev. Lett.* **86**, (2001) 971.
6. K. Starosta, in *Nuclei at the Limits*, edited by T.L. Khoo and D. Seweryniak, AIP Conf. Proc. **764**, (2005) 77.
7. S. Brant et al., *Phys. Rev. C* **69**, (2004) 017304.
8. J. Simpson, *Z. Phys. A* **358**, (1997) 139.
9. A. Dewald et al., *Z. Phys. A* **334**, (1989) 163.
10. G. Böhm, A. Dewald, P. Petkov and P. von Brentano, *Nucl. Instrum. Methods Phys. Res. A* **329**, (1993) 248.
11. P. Petkov et al., *Nucl. Phys. A* **640**, (1998) 293.
12. P. Petkov et al., *Nucl. Instrum. Methods Phys. Res. A* **431**, (1999) 208.
13. G. Winter, *Nucl. Instrum. Methods* **214**, (1983) 537.
14. T. Klemme et al., *Phys. Rev. C* **60**, (1999) 034301.
15. S. P. Roberts et al., *Phys. Rev. C* **67**, (2003) 057301.
16. D. Tonev et al., *Phys. Rev. Lett.* **96**, (2006) 052501.
17. D. Tonev et al.,*Phys. Rev. C* **76**, (2007) 044313.
18. K. Starosta et al., *Phys. Rev. C* **69**, (2002) 044328.
19. T. Koike et. al., *Phys. Rev. Lett.* **93**, (2004) 172502.
20. I. Ragnarsson et al.,*Hyperfine Interact.* **43**, (1988) 425.
21. S. Brant, D. Tonev, G. de Angelis, A. Ventura, submitted in *Phys. Rev. Lett.*